Compact Slow-Light Integrated Silicon Electro-Optic Modulators With Low Driving Voltage

Stephen R. Anderson, Amir Begović, Hao Jiang, and Z. Rena Huang, *Member, IEEE*

***Abstract*— In this work, we report two slow-light enhanced silicon optical modulators with electro-optic (EO) phase shifter lengths of 500 μm and 150 μm that were fabricated using the AIM Photonics foundry. Tunable power splitters give a threefold increase in the extinction ratio (ER). An eye diagram operating at 10 Gbps was achieved using a very low signal voltage of V_{pp} = 500mV. The energy per bit is 57.5 fJ/bit and 45 fJ/bit for the 500 μm and 150 μm modulators, respectively. The nonlinearity of the devices were measured yielding spur-free dynamic range of 113.2 dB/Hz$^{2/3}$. The 150 μm length MZM is among the smallest optical modulators using Bragg gratings for slow light ever reported and results in an estimated modulation efficiency of 0.33 V·cm.**

***Index Terms*— Photonics, slow-light, grating, modulator, RF-photonics, low-power.**

I. Introduction

INTEGRATED Si electro-optic (EO) modulators have been extensively studied in the last two decades, and are widely used in many applications such as optical communication for fiber network, optical interconnects and chip-scale photonic neural networks [1], [2]. However, depletion type Si EO Mach-Zehnder modulators (MZMs) with fast carrier response times have long phase shifter (PS) lengths, typically 1-4 mm [3], which require traveling wave electrodes (TWEs) to drive the RF signals along the PS. This issue can be addressed by integrating slow-light (SL) structures using line-defect photonic crystal waveguides (PCWs) [4] or transmission type Bragg gratings [5] to effectively enhance the light-matter interaction, thereby improving modulation efficiency and ultimately allowing reduction in PS length. While PCW optical modulators have demonstrated high group indices, they can be challenging in manufacturing scalability, whereas Bragg grating PSs with foundry-friendly critical dimensions of ∼150 nm offer a good compromise in device performance and manufacturing scalability.

In this work, we investigate two slow light modulators (SLMs) with PS lengths of 500 μm (SLM A) and 150 μm (SLM B). As the EO PS is short, a lumped element model can be used for the electrode design, rather than requiring complex TWEs [6]. The trade-off of reducing the PS length is degraded extinction ratio (ER), which impacts the transmission bit rate in an optical link. To address the trade-off, we use uneven power splitting of an unbalanced MZM to reduce insertion loss as well as maximizing the ER of the modulator. Most reported SLMs were tested with peak-to-peak driving voltages (V_{pp}) greater than 3 V [4], [5], [6] while modulator driver circuits realized by low-power CMOS often prefer $V_{pp} < 1$ V. Therefore, in this work we focus on using very low V_{pp} signals of 500 mV for the bit rate measurements. An optical link dominated by modulator nonlinearity can be characterized by spur-free dynamic range (SFDR). A SFDR of a SLM optical link using a PS length of 200 μm reported 104 dB/Hz$^{2/3}$ without Kerr effect [5]. In this work, our measurement shows that the 3rd order nonlinearity can be cancelled with proper choice of wavelength yielding a high SFDR of 113.2 dB/Hz$^{2/3}$. The reported monolithic Si SLM with small footprint and low driving voltage offers an attractive solution for low-cost and high-density integration of Si modulators for various applications.

II. Slow-Light MZM Structure

The schematics of the SLMs are depicted in Fig. 1. SLM A uses a thermo-optic switch (TOS) to adjust the optical power splitting ratio while SLM B utilizes a Y-splitter with even power splitting. A thermal PS is placed in either arm of the SLM for quadrature point tuning in the SFDR measurement. All devices are fabricated at American Institute of Manufacturing Photonics (AIM Photonics) foundry by their multi-project wafer (MPW) process.

The grating arm is apodized with a super-Gaussian profile for gradual mode matching from the fast light to the slow light region. Details of the grating parameters have been characterized in our previous work [7]. The key waveguide dimensions are H_f = 220 nm, W_c = 400 nm, and H_s = 110 nm. SLM A has grating width (W_g) of 800 nm while a W_g of 1.5 μm is set for SLM B. Periods of 290 nm

Manuscript received 16 February 2023; revised 18 April 2023; accepted 27 April 2023. Date of publication 4 May 2023; date of current version 22 May 2023. This work was supported in part by the U.S. Department of Defense Army Research Laboratory (ARL) under Grant W911NF-19-2-0170 and in part by the American Institute of Manufacturing (AIM) Photonics. The work of Stephen R. Anderson was supported by the DoD SMART Scholarship Program and the Army Research Laboratory. The work of Amir Begović was supported by the American Institute of Manufacturing (AIM) Photonics. *(Stephen R. Anderson and Amir Begović contributed equally to this work.) (Corresponding author: Z. Rena Huang.)*

Stephen R. Anderson is with the Department of Electrical, Computer and Systems Engineering, Rensselaer Polytechnic Institute, Troy, NY 12180 USA, and also with the Army Research Laboratory, Sensors and Electron Devices Directorate, Adelphi, MD 20783 USA (e-mail: anders8@rpi.edu).

Amir Begović and Z. Rena Huang are with the Department of Electrical, Computer and Systems Engineering, Rensselaer Polytechnic Institute, Troy, NY 12180 USA (e-mail: begova@rpi.edu; huangz3@rpi.edu).

Hao Jiang is with the School of Engineering, San Francisco State University, San Francisco, CA 94132 USA (e-mail: jianghao@sfsu.edu).

Color versions of one or more figures in this article are available at https://doi.org/10.1109/LPT.2023.3273178.

Digital Object Identifier 10.1109/LPT.2023.3273178

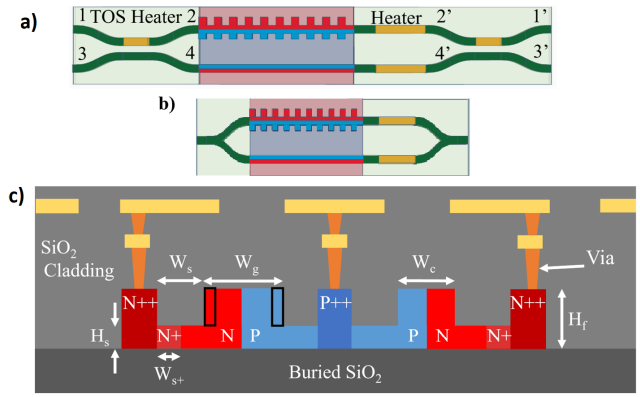

Fig. 1. a) The top view of SLM A: Thermo-optic switches adjust the input and output splitting ratio. Another heater in-line with the modulator arms is used for additional phase adjustment or setting the modulator in quadrature. b) Top view of SLM B: Y-branches are used instead of thermo-optic switches. c) Modulator cross-section: P and N type doping are represented by blue and red regions of doped silicon. The mode propagation direction is along the z axis (into the page). For SLM B, the P doping level is replaced with P+ doping.

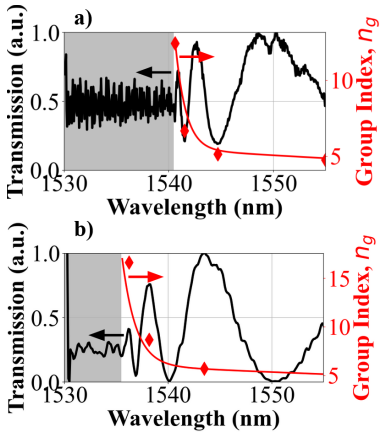

Fig. 2. a) Spectrum of SLM A and b) SLM B. The gray shaded region indicates the extent of the stopband of the gratings. SLM A has a stop band width of 25 nm centered at 1527.5 nm while SLM B has a stop band width of 45 nm centered at 1512.5 nm.

and 282 nm are used for SLM A and B, respectively, with both using a 50% duty cycle. Half width Si slab is the standard process of AIM. A rather long $W_s = 2.45$ µm is design to confine the optical field within the rib waveguide. A higher doping is applied along a width $W_{s+} = 1.25$ µm to reduce the series resistance without impinging on the optical mode. Both SLMs use lateral PN junctions. The doping in both the N and P region of SLM A is $\sim 10^{18}$ cm^{-3} while the P doping of SLM B is elevated to $\sim 10^{19}$ cm^{-3}, allowing for an ultra-short PS.

III. Results and Discussion

A. Group Index and Modulation Efficiency Characterization

We first measured the SLM power transmission and characterized the group indices using an interference method [8]. As shown in Fig. 2, near the photonic band gap, both devices exhibit a stronger slow light effect. The highest measured group index is ~16.

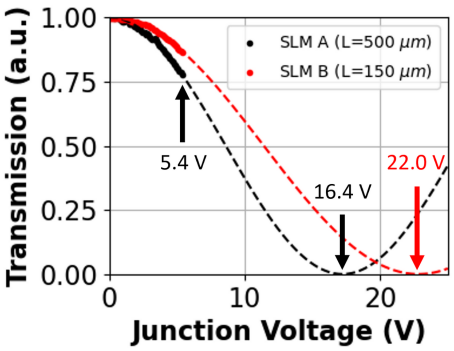

Fig. 3. Sinusoidal extrapolation of measured data for the SLMs, used to estimate V_π. Data leading into the junction breakdown regime is ignored. The wavelengths used are 1540.72 nm and 1536.40 nm for SLM A and B, respectively.

Modulation efficiency is characterized by the $V \cdot L$ product, but for a short PS, it may not be possible to attain a π phase shift without pushing the junction bias to its breakdown regime. The measured V_π for SLM A is 7.7 V, while the junction breakdown occurs at 7.8 V. We attribute the measured V_π to the large carrier injection at the onset of avalanche break down. As such, we discarded the measured $V_\pi = 7.7$ V and explored alternative methods to estimate the modulator efficiency for ultra-short PS devices when the junction is biased well under breakdown.

Several methods to estimate modulator efficiency for short PS devices were reported [9], [10]. In this work, we utilized a curve fit method for estimating $V \cdot L$. SLM output intensity data measured up to V = 5.4 V was used as the baseline for curve fitting to a sinusoidal response, as shown in Fig. 3. Though a Si MZM has multiple sources of nonlinearities, the sinusoidal response of the transfer function is predominant among all nonlinearities when the PS is sufficiently long. Using the curve fit method, we estimated $V \cdot L = 0.82$ V·cm for SLM A. To validate this result, we characterized a separate SLM with identical doping and a PS length of 2 mm and obtained a measured V_π of 4.5 V leading to $V_\pi \cdot L = 0.90$ V·cm, close to the estimated $V \cdot L$ for SLM A. Following this method, SLM B is estimated to have $V \cdot L = 0.33$ V·cm for a π phase shift. The higher modulation efficiency in SLM B is attributed to the increased doping concentration as well as a larger W_g. Modulation efficiency characterization was performed for the SLMs at the first peak transmission wavelength adjacent to the photonic band gap.

B. Insertion Loss and Extinction Ratio

The extinction ratio of the SLM is influenced by various factors such as the phase shifter length, loss, DC bias point, driving voltage V_{pp}, and choice of operation wavelength. To estimate the insertion loss, we began by measuring the on-chip Ge PD response which takes into account the end-fire fiber-to-chip coupling loss (~5.5 dB), on-chip mode converter loss, and routing waveguide propagation loss. This allows us to de-embed these losses when measuring the SLMs. The estimated total insertion loss for SLM A and B is 9.4 dB and 6.4 dB, respectively, measured in the slow light wavelengths

of 1540 and 1538 nm. This includes the active thermal splitter loss (∼2 dB) and thermal PS loss (∼0.5 dB). The characterization was carried out at the strong SL regime (n_g∼16) so the SL induced increased scattering loss is properly accounted in the loss measurement. Though SLM B has higher doping, its shorter PS length gives lower total loss comparing to the longer device.

An unbalanced SLM design where the reference arm is a plain ridge waveguide was adopted in this work. This lowers the total insertion loss compared to a balanced configuration. The SL arm has a higher propagation loss than the reference arm. For SLM A, the static ER under uneven splitting ratios of 20%, 50%, 60%, 75% and 87% are characterized for the cases of a large V_{pp} at 4 V and a small V_{pp} at 500 mV. The TOS introduces a splitting ratio dependent phase difference at port 1 and 2 (see Fig. 1a). This phase difference is carefully compensated by the thermal PS in the MZM SL arm. Compared with even splitting at 50%, a threefold improvement in the static ER was demonstrated with a splitting ratio of 87% for both V_{pp} cases.

However, power consumption scales with V_{pp}^2, while the ER is degraded with reduced V_{pp}, which adversely impacts the SLM transmission bit rate. Hence, it is essential to carry out a holistic design in SLM power consumption and bit rate. For SLM A, when the V_{pp} changes from 4 V to 500 mV at a splitting ratio of 87%, the ER reduces from 14.5 dB to 2.5 dB.

For SLM B, equal power splitting/combining using Y-junctions was used. Due to the large difference in propagation loss in SL arm and ridge waveguide reference arm, a best static ER = 2.2 dB was obtained for V_{pp} = 500 mV near the photonic band edge.

C. SLM Bit Rate Characterization

Due to the short PSs in both SLMs, lumped elements are used in electrodes design [6]. The total electrical bandwidth is determined by both the RC time and the photon lifetime. The capacitance of SLM A is measured to be ∼0.92 pF at a −3 V bias, while that of SLM B is ∼0.72 pF at the same bias, with slab resistances calculated to be 6 Ω and 2 Ω, respectively. The estimated energy per bit, $E_{bit} = \frac{1}{4}CV_{pp}^2$ is 57.5 fJ/bit for SLM A and 45 fJ/bit for SLM B [1]. We attribute the low energy consumption to the short PS length and ultra-low driving voltage of 500 mV_{pp}. The electrical bandwidth of both devices exceeds our equipment capable speed of 6.5 GHz.

The eye diagrams of the SLMs were measured under a differential drive of V_{pp} = 500 mV, and demonstrated 7 Gbps for SLM A and 10 Gbps for SLM B. The eye diagrams are plotted in Figure 4. Both SLMs are not 50 Ω terminated, so impedance mismatch to the testing equipment significantly limits the tested bit rates. In practical applications, the modulator driver circuit can be designed to have matched output impedance to the SLM.

D. RF Link Linearity Characterization

The linearity of the SLM is characterized in an RF photonic link by two-tone intermodulation distortion measurement at

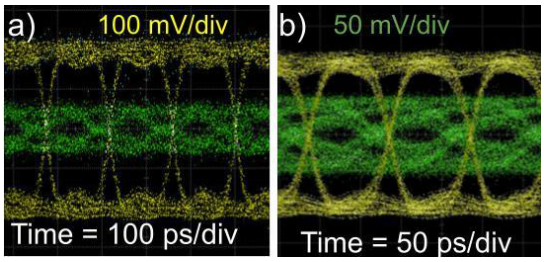

Fig. 4. Green data represents SLM output; the yellow data is the input signal directly measured from the AWG. a) Eye diagram of SLM A operating at 7 Gbps. The input signal is 500 mV_{pp} differentially driven signal at −3 V DC voltage and laser wavelength is fixed at 1543.32 nm. b) Eye diagram operating at 10 Gbps for SLM B. The input signal is 500 mV_{pp} differentially driven signal at −6 V DC voltage and laser wavelength is fixed at 1540.4 nm.

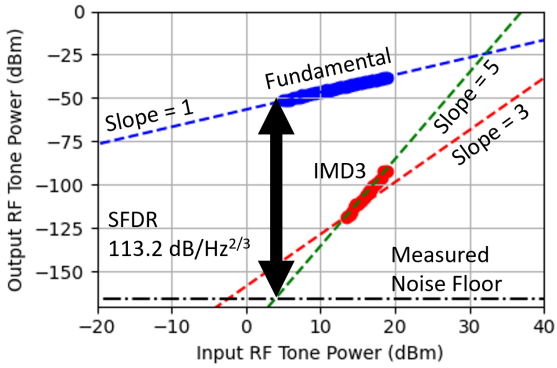

Fig. 5. The two-tone test applied to SLM A. The dashed curves represent ideal slopes of 1, 3 and 5. The choice of slow-light wavelength (λ = 1542.16 nm) eliminates the 3rd order distortions, and leaves only the 5th order nonlinear.

RF frequencies near 500 MHz. The measurement setup was reported in a previous work [7]. For the test of SLM A, the output from the modulator is terminated with an off-chip commercial PD while for SLM B, an on-chip PD provided in the AIM PDK is used. The highest SFDR of SLM A is measured to be 113.2 $dB/Hz^{2/3}$. The two-tone diagram for SLM A is plotted in Fig. 5. This computation of SFDR assumes that the IMD tone scales with the 3rd order, while the IMD3 distortion can be eliminated at the proper wavelength choice, leaving only the 5th-order nonlinear component. The combination of TOS splitting ratio, and the choice of operating wavelength in the slow-light region, offers an extra degree of freedom necessary to cancel the 3rd-order distortion. The linearity of SLM B is reduced because of the nonlinear response of the on-chip AIM PD. The probe circuitry on the AIM PD also has noticeable electromagnetic crosstalk from the nearby MZM electrodes. This combination of factors limits the linearity of SLM B to 99 $dB/Hz^{2/3}$.

IV. Conclusion

Two slow-light modulators with PS of 500 μm and 150 μm were studied. The estimated modulation efficiency of SLM A is 0.82 V·cm, while SLM B's modulation efficiency is 0.33 V·cm. The better efficiency in SLM B is attributed to an increase in the junction doping and larger grating width. Total insertion losses of the SLMs are characterized at 9.4 dB and 6.4 dB for SLMs A and B, respectively. Despite SLM B having

close to 10^{19} cm^{-3} doping, the shorter PS results in lower total insertion. We also studied uneven splitting ratios in SLM A and demonstrated threefold improvement in ER. We used a lumped element model in the SLM electrode and achieved bit rates of 7 Gbps and 10 Gbps for NRZ signals using differential driving on the SLMs, with power consumptions of 57.5 fJ/bit and 45 fJ/bit for SLM A and B, respectively. The speed is limited by impedance mismatch between the characterization equipment and devices. The dispersion characteristics of the SLM offers wavelength dependent cancellation of the 3rd order intermodulation component, resulting in the highest tested SFDR of 113.2 dB/$Hz^{2/3}$ for SLM A.

REFERENCES

[1] J. Witzens, "High-speed silicon photonics modulators," *Proc. IEEE*, vol. 106, no. 12, pp. 2158–2182, Dec. 2018.

[2] C. Han, M. Jin, Y. Tao, B. Shen, and X. Wang, "Recent progress in silicon-based slow-light electro-optic modulators," *Micromachines*, vol. 13, no. 3, p. 400, Mar. 2022.

[3] M. Aamer et al., "10 Gbit/s error-free DPSK modulation using a push–pull dual-drive silicon modulator," *Opt. Commun.*, vol. 304, pp. 107–110, Sep. 2013.

[4] Y. Hinakura, D. Akiyama, H. Ito, and T. Baba, "Silicon photonic crystal modulators for high-speed transmission and wavelength division multiplexing," *IEEE J. Sel. Topics Quantum Electron.*, vol. 27, no. 3, pp. 1–8, May 2021.

[5] P. Xia et al., "High linearity silicon DC Kerr modulator enhanced by slow light for 112 Gbit/s PAM4 over 2 km single mode fiber transmission," *Opt. Exp.*, vol. 30, no. 10, pp. 16996–17007, 2022.

[6] M. Xu and X. Cai, "Advances in integrated ultra-wideband electro-optic modulators [invited]," *Opt. Exp.*, vol. 30, no. 5, pp. 7253–7274, 2022.

[7] S. R. Anderson, A. Begovic, and Z. R. Huang, "Integrated slow-light enhanced silicon photonic modulators for RF photonic links," *IEEE Photon. J.*, vol. 14, no. 4, pp. 1–6, Aug. 2022.

[8] E. Dulkeith, F. Xia, L. Schares, W. M. J. Green, and Y. A. Vlasov, "Group index and group velocity dispersion in silicon-on-insulator photonic wires," *Opt. Exp.*, vol. 14, no. 9, pp. 3853–3863, 2006.

[9] O. Jafari, W. Shi, and S. Larochelle, "Mach–Zehnder silicon photonic modulator assisted by phase-shifted Bragg gratings," *IEEE Photon. Technol. Lett.*, vol. 32, no. 8, pp. 445–448, Apr. 15, 2020.

[10] Y. Di, P. Gardner, and H. Ghafouri-Shiraz, "Methods for measuring the RF half-wave voltage of $LiNbO_3$ optical modulators," *Microw. Opt. Technol. Lett.*, vol. 46, no. 5, pp. 440–443, Sep. 2005.

[11] B. Murray, C. Antony, G. Talli, and P. D. Townsend, "Predistortion for high-speed lumped silicon photonic Mach–Zehnder modulators," *IEEE Photon. J.*, vol. 14, no. 2, pp. 1–11, Apr. 2022.

[12] J. R. G. Sugesh and A. Sivasubramanian, "Modelling and analysis of a corrugated PN junction phase shifter in silicon MZM," *Silicon*, vol. 14, no. 6, pp. 2669–2677, Apr. 2022.